A R C H I V E S O F M E T A L L U R G Y A N D M A T E R I A L S
Volume 59 2014 Issue 4
DOI: 10.2478/amm-2014-0246

C. RAPIEJKO*, B. PISAREK*, E. CZEKAJ**, T. PACYNIAK*

ANALYSIS OF AM60 AND AZ91 ALLOY CRYSTALLISATION IN CERAMIC MOULDS BY THERMAL DERIVATIVE ANALYSIS (TDA)

ANALIZA KRYSTALIZACJI STOPÓW AM60 I AZ91 W FORMIE CERAMICZNEJ METODĄ ANALIZY TERMICZNO-DERYWACYJNEJ (ATD)

The work presents the test results of the crystallisation and cooling of magnesium alloys: AM60 and AZ91, with the use of the TDA method. The tested alloys were cast into ceramic shells heated up to 180°C, produced according to the technology of the shell production in the investment casting method. The TDA method was applied to record and characterize the thermal effect resulting from the phase transformations occurring during the crystallisation of magnesium alloys. The kinetics and dynamics of the thermal processes of the crystallisation of AM60 and AZ91 in the ceramic shells were determined. Metallographic tests were performed with the use of an optical microscope as well as scanning microscopy, together with the EDS chemical analysis of the phases present in the tested casts. A comparison of these test results with the thermal effect recorded by way of the TDA method was made.

Keywords: innovative casting materials and technologies, crystallisation, magnesium alloys, light alloys, TDA method

W pracy przedstawiono wyniki badań krystalizacji i stygnięcia stopów magnezu: AM60 i AZ91 przy użyciu metody ATD. Badane stopy zalewano do form ceramicznych podgrzanych do temperatury 180°C, wykonanych zgodnie z technologią wytwarzania form w metodzie traconych modeli. Przy pomocy metody ATD zarejestrowano i wyznaczono charakterystyczne efekty cieplne wynikające z przemian fazowych zachodzących podczas krystalizacji badanych stopów magnezu. Określono kinetykę i dynamikę procesów cieplnych krystalizacji stopów AM60 i AZ91 w formach ceramicznych. Przeprowadzono badania metalograficzne przy pomocy mikroskopu optycznego oraz mikroskopii skaningowej wraz z analizą chemiczną EDS występujących faz w badanych odlewach. Porównano wyniki tych badań z efektami cieplnymi zarejestrowanymi metodą ATD.

1. Introduction

The crystallisation and cooling tests on the alloys by the thermal derivative analysis has been known for years. This method allows for the determination of the kinetics and dynamics of the thermal processes of metal crystallisation. It is applied for the analysis of the alloys of both the ferrous [1,2] and the non-ferrous metals such as bronzes [3,4] or aluminium alloys [5-7]. In the recent years, tests of the crystallisation and cooling of magnesium alloys has been initiated. They have been normally performed in samplers – metal crucibles [8,9], which rapidly give back the heat. These tests are close to the real conditions present in the casting mould made of metal. As regards magnesium alloys, more and more often, they are applied in the production of casts by the investment casting method in ceramic shells [10-12]. The ceramic shells characterize in a much lower heat conductivity coefficient, and so the solidification and the crystallisation process is different than that in the metal moulds. In the world literature, there are no reports on the solidification and cooling process tests of magnesium alloys in a ceramic shell used in the investment casting method.

The aim of this work was to test the solidification and crystallisation of magnesium alloys: AM60 and AZ91 in the ceramic ATD10C-PŁsampler developed at the Department of Materials Engineering and Production Systems of Lodz University of Technology by the TDA method.

2. Test methodology

The TDA method was applied to test the solidification and crystallisation process of magnesium alloys: AM60 and AZ91, produced in specially designed ceramic samplers. The ceramic shells of the samplers were made according to the technology of ceramic shell production in the investment casting method (lost wax method) applied in the obtaining of aluminium alloy casts [13]. The construction of the applied TDA samplers is presented in Figure 1.

* LODZ UNIVERSITY OF TECHNOLOGY, DEPARTMENT OF MATERIALS ENGINEERING AND PRODUCTION SYSTEMS, 1 STEFANOWSKIEGO STR., 90-924 ŁÓDŹ, POLAND
** FOUNDRY RESEARCH INSTITUTE, 73 ZAKOPIAŃSKA STR., 34-120 KRAKÓW, POLAND

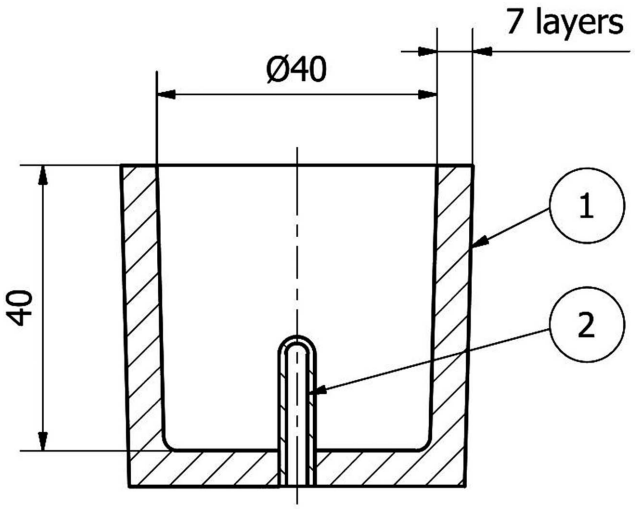

Fig. 1. Construction of TDA samplers: 1 – Shell of ATD10C-PŁmould, 2 – Quartz tube unilaterally vaulted

The ceramic shells of the TDA samplers were made of refractory REFRACORSE flour and sands. The shells consisted of 7 coatings made in mixers and in a fluidizer, at the „Armatura" Foundry in Łódź, Poland. Each coating was created as a result of applying a binder on the wax model and next covering it with quartz sand of a particular granularity. Figure 2 presents the ceramic ATD10C-PŁsampler used during the tests.

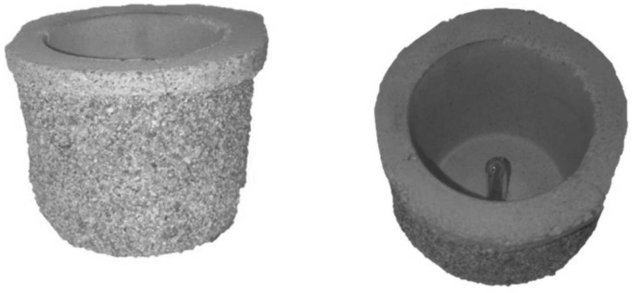

Fig. 2. Ceramic ATD10C-PŁsampler

The configuration and the type of the used coatings is presented in Table 1.

TABLE 1

Coating characteristics

Coating no.	Viscosity [s]	Binder type	Sand granularity [mm]
1	38	Ludox	0.1-0.3
2	20	Ludox	0.1-0.3
3	17	Ethyl silicate	0.2-0.5
4	18	Ethyl silicate	0.5-1.0
5	19	Ludox	0.5-1.0
6	18	Ethyl silicate	0.5-1.0
7	20	Ethyl silicate	0.5-1.0

After the desiccation, a model mass was melted from the ceramic shell in an autoclave at 150°C. Next, the shell was reinforced at 960°C in a tunnel furnace. After the burning, the ceramic samples were cooled down to 180°C, and then liquid 800°C±5°C metal was cast on them.

The chemical composition of the AM60 alloy is presented in Table 2.

TABLE 2

Chemical composition of alloy AM60

Chemical composition, % wt.							
Mg	Al	Zn	Mn	Si	Fe	Cu	Ni
93.697	6	0	0.23	0.05	0.004	0.008	0.001

The chemical composition of the AZ91 alloy is shown in Table 3.

TABLE 3

Chemical composition of alloy AZ91

Chemical composition, % mas							
Mg	Al	Zn	Mn	Si	Fe	Cu	Ni
90.027	9	0.8	0.1	0.05	0.004	0.008	0.001

The metal was melted in a laboratorial crucible resistance furnace of 5 kg capacity. The crucible was made of S235JRG2 steel – standard PN-EN 10025-2:2005. Inside the furnace, protective gas atmosphere was used which consisted of an Ar + SF_6 mixture with the pressure of 0.15-0.20 MPa. The gas flow equalled 10 cm^3/min for SF_6 and 500 cm^3/min for Ar.

The recording of the TDA characteristics was performed at a working station, whose scheme can be seen in Figure 3.

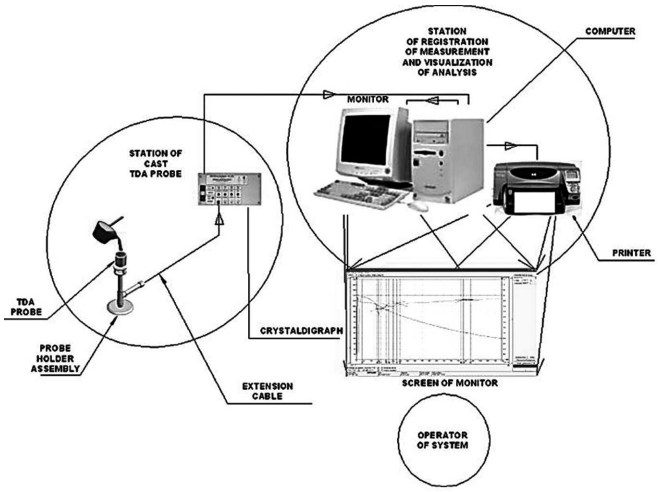

Fig. 3. Scheme of the TDA measuring station

One of the elements of the working station is a TDA stand, in which a measuring thermoelement type S was installed (Pt-PtRh10). The thermoelement was connected with an analogue-digital converter, Crystaldigraph, which converted the voltage signal into a frequency one, which was then recorded by the computer. The evaluation of the cooling (t=f(τ)), kinetics (dt/dτ =f '(τ)) and dynamics ($d^2t/d\tau^2$ = f "(τ)) of the crystallisation processes was performed by the TDA method. On the derivative curve dt/dτ =f '(τ) the following thermal effects were marked for magnesium alloys:

AM60 and AZ91:

Pk-A-D – crystallisation of primary α_{Mg} phase ($L \rightarrow L+\alpha_{Mg}$),

D-E-F-H – crystallisation of $\alpha_{Mg} + \gamma(Mg_{17}Al_{12})$ eutectic ($L \rightarrow \alpha_{Mg} + \gamma(Mg_{17}Al_{12})$).

In the description of the characteristics of the thermal processes occurring during the primary crystallisation, the following quantities were applied:

- the temperature of the alloy (liquid metal), with the recording of the characteristic points t, °C,
- the value of the first derivative of the temperature after the time for these points dt/dτ, °C/s,
- the value of the tangent of the inclination angle of the straight line at the interpolated interval between the characteristic points $tg(\alpha) \approx d^2t/d\tau^2$, °C/s^2,
- the time which passed from the beginning of the measurement of the occurrence of the characteristic points on the derivative curve (crystallisation curve) τ, s.

In order to demonstrate the particular phases in the microstructure, the microsections were etched with a reagent of the following composition: 1 ml acetic acid, 50 ml distilled water and 150 ml ethyl alcohol [14]. The microstructure of the samples of magnesium and the examined alloys was observed by means of the Nikon Eclipse MA200 optical microscope.

For the identification of the chemical composition at the particular points of the cast's microstructure, the samples were observed with the use of scanning microscopy, by means of the Hitachi S-4200 scanning microscope of 15 kV accelerating voltage, together with an EDS analyser.

3. Result description

3.1. Test results for AM60 magnesium alloy

Figure 4 presents the TDA characteristics of the AM60 alloy solidifying in the ceramic ATD10C-PŁsampler. On the derivative curve (dt/dτ), points Pk, A, D and E determine the thermal effect of the crystallisation of α_{Mg} phase within the volume of the sampler; E, F and H determine the thermal effect of the crystallisation of the $\alpha_{Mg} + \gamma(Mg_{17}Al_{12})$ eutectic. After the metal is cooled below the equilibrium liquidus temperature, the grains of the α_{Mg} phase nucleate and grow at the actual liquidus temperature tA=610°C. The intensity of the cooling rate change at the initial stage of the crystallisation of the α_{Mg} phase's grains is slightly lower than the crystallisation of magnesium and it equals ZPk=206.40·10^{-3}°C/s^2; on the cooling curve t=f(τ), there is no recalescence of the alloy's temperature during the cooling process. After reaching the maximum thermal effect of the α_{Mg} phase's crystallisation at point A, the intensity of the cooling rate change decreases to ZA=-24.33·10^{-3}°C/s^2. The crystallisation of the AM60 alloy after the maximum thermal effects have been reached (point A), but not the whole volume of the liquid alloy crystallizes as α_{Mg} phase. On the derivative curve, during the crystallisation of the α_{Mg} phase in the AM60 alloy, the thermal effect Pk-A-D, the duration time of this effect equals SK_{Pk-D} = 129.6 s. The thermal effect Pk-A-D includes the stage of intense nucleation and growth of the α_{Mg} phase; at the interval between points D and E, the kinetics of the thermal processes (dt/dτ) of the growth of the α_{Mg} phase slightly decreases. The dynamics of the thermal processes around point D changes: ZD=-2.95·10^{-3}°C/s^2 and ZE=0.56·10^{-3}°C/s^2, respectively. At this stage, at the front of the crystallisation of the α_{Mg} phase in the liquid alloy, the Al concentration slowly increases, which in consequence leads to the nucleation and growth of the $\alpha_{Mg} + \gamma(Mg_{17}Al_{12})$ eutectic. After the cooling of the liquid alloy below the equilibrium temperature of the eutectic transformation at the actual transformation temperature tF=437.5°C, the $\alpha_{Mg} + \gamma(Mg_{17}Al_{12})$ eutectic nucleates and grows. The actual temperature of the eutectic crystallisation in the tested alloy is higher than the equilibrium temperature in the Mg-Al system (Teut= 437°C), which is caused by the fact that, in the AM60 alloy, beside the basic components such as Mg and Al, also present are other elements, especially 0,23% Mn, which affects the increase of this temperature. Thus one can presume that, in such a complex equilibrium system Mg-Al-Mn-other elements, the temperature of the eutectic transformation is higher than the actual temperature recorded in the TDA sampler. The crystallisation process of the $\alpha_{Mg} + \gamma(Mg_{17}Al_{12})$ eutectic runs with significant dynamics of the thermal processes of crystallisation, both before (ZF=71,91·10^{-3}°C/s^2) and after the maximum (ZH=-66,97·10^{-3}°C/s^2) of these effects (point F). The AM60 alloy solidified within the volume of the ATD10C-PŁsampler at time SK_{Pk-H} = 291.2 s, of which the crystallisation of the α_{Mg} phase lasted SK_{Pk-E} = 248.8 s, and the crystallisation of the $\alpha_{Mg} + \gamma(Mg_{17}Al_{12})$ eutectic – SK_{E-H} = 42.4 s.

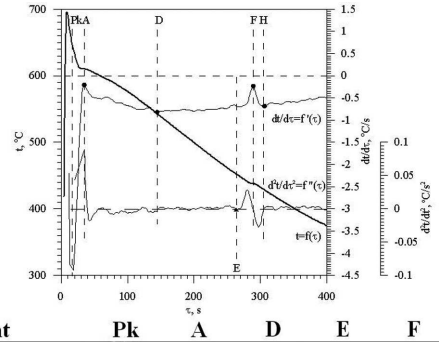

Point	Pk	A	D	E	F	H
τ, s	14.6	34.6	144.2	263.4	289	305.8
t, °C	659.0	610.2	542.9	452.3	437.5	428.3
dt/dτ, °C/s	-5.49	-0.21	-0.82	-0.00	-0.23	-0.68
Z≈d²t/dτ², *10^{-3} °C/s^2	206.4	-24.33	-2.95	0.56	71.91	-66.97

Fig. 4. TDA characteristics of the AM60 alloy solidifying in the ceramic TDA sampler

Figure 5 (a,b) shows the microstructure of the AM60 alloy solidifying in the ATD10C-PŁsampler. The microstructure of the AM60 alloy consists of the following phases: α_{Mg}+ eutectic ($\alpha_{Mg} + \gamma(Mg_{17}Al_{12})$).

Figure 6 presents an electron microscope photograph of the microstructure of the AM60 solidifying in the ceramic ATD10C-PŁsampler, with marked areas (1-3) of the local analysis of the chemical composition. The diagrams of the chemical composition analysis at points 1, 2 and 3 of the microstructure of the AM60 alloy solidifying in the ceramic sampler are shown in Figure 7, whereas Table 4 presents the results of the chemical composition analysis of the AM60 alloy at the examined points.

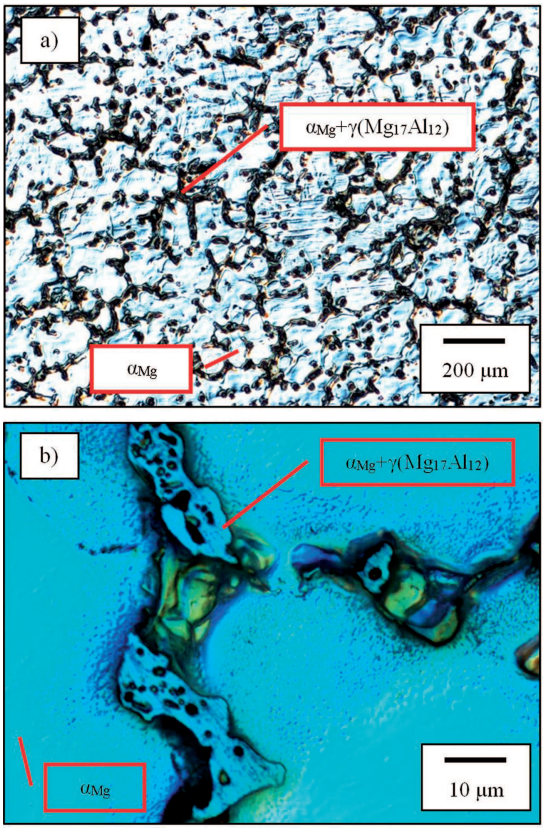

Fig. 5. Microstructure of the AM60 alloy solidifying in the ceramic TDA sampler

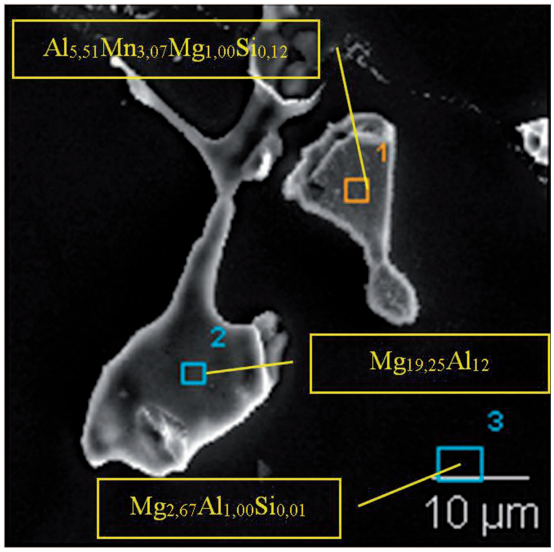

Fig. 6. Electron microscope photograph of the AM60 alloy solidifying in the ceramic ATD10C-PŁsampler

The surface of the tested AM60 alloy oxidizes relatively fast, and thus, the analysis at points 1-3 identified oxygen. The fluorine identified on a significant surface of the sample (point 3) probably originates from the liquids used during the preparation of the metallographic microsections. The Al concentration in the α_{Mg} phase equalled about 3.9% (Fig. 6, Fig. 7, Tab. 4: point 3). The magnesium-aluminium eutectic phase ($Mg_{17}Al_{12}$) has a higher content of magnesium atoms, similar to that of the $Mg_{19.5}Al_{12}$ phase (Fig. 6, Fig. 7, Tab. 4: point 2). The microstructure of the alloy showed the presence of precipitates of an aluminium-manganese intermetallic phase, type $Al_{5,51}Mn_{3,07}Mg_{1,00}Si_{0,12}$ (Fig. 6, Fig. 7, Tab. 4: point 1).

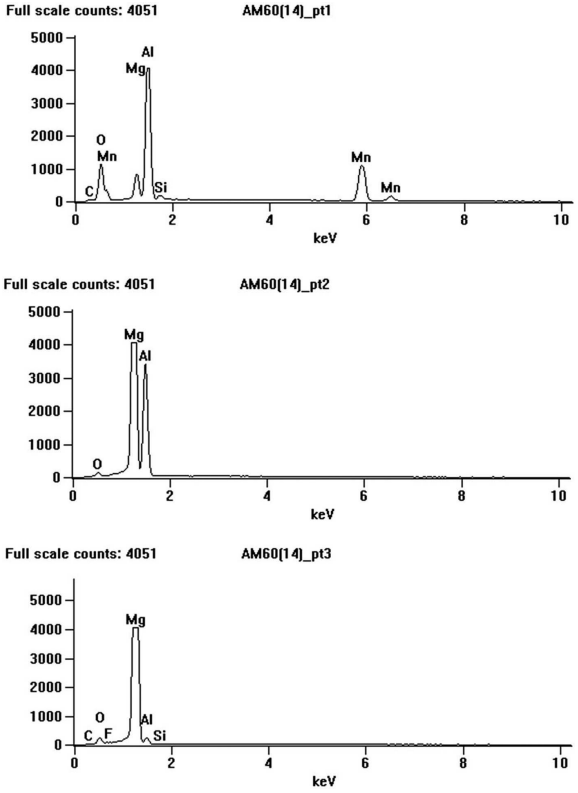

Fig. 7. Diagram of the chemical composition analysis at points 1-3 of the microstructure of the AM60 alloy solidifying in the ceramic ATD10C-PŁsampler

TABLE 4
Results of the chemical composition analysis of the AM60 alloy phases

Point of analysis	Element	Element concentration, %	
		Mass	Atomic
1	Mg	7.1	10.3
	Al	43.1	56.8
	Si	1.0	1.2
	Mn	48.8	31.6
2	Mg	59.1	61.6
	Al	40.9	38.4
	Si	–	–
	Mn	–	–
3	Mg	95.8	96.2
	Al	3.9	3.6
	Si	0.3	0.2
	Mn	–	–

3.2. Test results for AZ91 magnesium alloy

Figure 8 shows the TDA characteristics of the AZ91 alloy in the ceramic ATD10C-PŁsampler. On the derivative curve (dt/dτ), points Pk, A, D and E determine the thermal effect of the crystallisation of the α_{Mg} phase within the volume of the sampler; points E, F and H determine the thermal effect of the crystallized $\alpha_{Mg} + \gamma(Mg_{17}Al_{12})$ eutectic. After the cooling of the metal below the equilibrium liquidus temperature, the grains of the α_{Mg} phase nucleate and grow at the actual liquidus temperature tA=589.6°C. The observed decrease of the liquidus temperature in relation to that of the AM60 alloy is mainly caused by the 3% Al concentration in the AZ91 alloy and thus the shift of the alloy's chemical composition in the Mg-Al towards the eutectic point can be observed. The intensity of the cooling rate change at the initial stage of the grain crystallisation of the α_{Mg} phase is lower than that of the AM60 alloy and equals ZPk=159.99·10^{-3}°C/s^2. Similarly to the case of AM60, the cooling curve t=f(τ) does not include the temperature recalescence of the alloy during its cooling. After reaching the maximum thermal effects of the crystallisation of the α_{Mg} phase at point A, the intensity of the cooling rate change decreases to ZA=-50.23·10^{-3}°C/s^2. The crystallisation of the AZ91 alloy after the maximum thermal effects have been reached (point A) characterizes in slightly lower dynamics d^{2}t/dτ^2 of the thermal processes during the crystallisation of the α_{Mg} phase (Fig. 8) than the dynamics during the AM60 alloy's crystallisation (Fig. 4). Similarly to the AM60 alloy, not the whole volume of the liquid alloy crystallizes as the α_{Mg} phase. On the derivative curve, during the crystallisation of the α_{Mg} phase in the AZ91 alloy, the thermal effect Pk-A-D occurs. The duration time of this effect equals SK_{Pk-D} = 119.2 s and shorter than that of the AM60 alloy. The thermal effect Pk-A-D includes the stage of intense nucleation and growth of the α_{Mg} phase; at the interval between points D and E, the kinetics of the thermal processes (dt/dτ) of the growth of the α_{Mg} phase decreases more intensely than that of the AM60 alloy. The dynamics of the thermal processes around point D changes: ZD=-0.73·10^{-3} °C/s^2 and ZE=0.83·10^{-3}°C/s^2, respectively. At this stage, at the front of the crystallisation of the α_{Mg} phase in the liquid alloy, the Al concentration slowly rises, which, in consequence, leads to nucleation and growth of the $\alpha_{Mg} + \gamma(Mg_{17}Al_{12})$ eutectic. After the cooling of the liquid metal below the equilibrium temperature of the eutectic transformation at the actual transformation temperature tF=430.0°C, the $\alpha_{Mg} + \gamma(Mg_{17}Al_{12})$ eutectic nucleates and grows. The actual temperature of the eutectic crystallisation in the tested alloy is lower than the equilibrium temperature in the Mg-Al system (Teut= 437°C). This is caused by the fact that, in the AZ91 alloy, beside the basic components such as Mg and Al, also present are other elements, especially 0.1% Mn, which stimulates the temperature increase, and 0.8% Zn, which lowers the temperature. And so, one can presume that, in such a complex equilibrium system Mg-Al-Zn-Mn-other elements the temperature of the eutectic transformation is lower than the actual temperature recorded in the TDA sampler, as the effect of Zn on the eutectic transformation temperature is probably stronger than that of Mn. Similarly to the case of the AM60 alloy, the crystallisation process of the $\alpha_{Mg} + \gamma(Mg_{17}Al_{12})$ eutectic runs with slightly lower crystallisation dynamics of the thermal processes than that of the AM60 alloy, both before (ZF=71.75·10^{-3}°C/s^2) and after (ZH=-35.20·10^{-3}°C/s^2) the maximum of these effects (point F). In the AZ91 alloy, the thermal effect E-F-H formed by the eutectic's crystallisation is higher and it occurs after a longer time than that in the case of the AM60 alloy. The AZ91 alloy solidified within the volume of the ATD10C-PŁsampler in time SK_{Pk-H} = 276.8 s, of which the crystallisation of the α_{Mg} phase lasted SK_{Pk-E} = 218.4 s, and that of the $\alpha_{Mg} + \gamma(Mg_{17}Al_{12})$ eutectic – SK_{E-H} = 58.4 s.

Due to the fact that, in comparison to AM60, in the case of AZ91, a higher amount of the liquid alloy crystallizes as an eutectic, whose crystallisation process characterizes in high dynamics of the thermal processes, both before and after the thermal effect maximum.

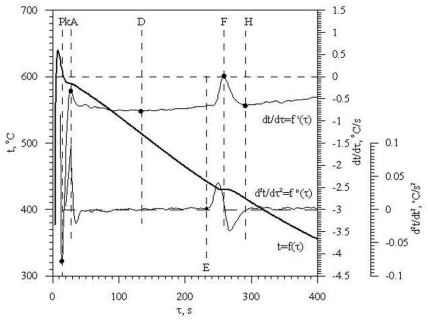

Point	Pk	A	D	E	F	H
τ, s	13.8	27.4	133.0	232.2	258.6	290.6
t, °C	613.3	589.3	514.7	442.2	430.0	416.6
dt/dτ, °C/s	-4.17	-0.33	-0.78	-0.65	0.01	-0.66
Z≈d²t/dτ², *10^{-3} °C/s²	159.99	-50.23	-0.73	0.83	71.75	-35.20

Fig. 8. TDA characteristics of the AZ91 alloy solidifying in the ceramic ATD10C-PŁsampler

Figure 9 (a,b) shows the microstructure of the AZ91 alloy solidifying in the ATD10C-PŁsampler. The microstructure of the AZ91 alloy consists of the following phases: α_{Mg}+ eutectic ($\alpha_{Mg} + \gamma(Mg_{17}Al_{12})$).

Figure 10 presents an electron microscope photograph of the microstructure of the AZ91 alloy solidifying in the ceramic ATD10C-PŁsampler, with marked areas (1÷4) of the local analysis of the chemical composition. The diagrams of the chemical composition analysis at points 1÷4 of the microstructure of the AZ91 alloy solidifying in the ceramic sampler are presented in Figure 11, whereas Table 5 shows the results of the chemical composition analysis at the examined points of the AZ91 alloy.

The surface of the tested sample of the AZ91 alloy, similarly to that of AM60 alloy, oxidizes relatively fast, and thus the observation of points 1÷4 of the analysis stated the presence of oxygen. In the $\alpha_{Mg,}$ phase, the Al concentration equals about 4.4%, and that of Si- about 0.3% (Fig. 10, Fig. 11, Tab. 5: point 3). The Mg-Al equilibrium eutectic phase ($Mg_{17}Al_{12}$) has an additional content of Zn atoms, similarly to the $Mg_{17,36}Al_{12,00}Zn_{0,42}$ phase (Fig. 10, Fig. 11, Tab. 5: point 1). In the fine lamellar eutectic of the $\alpha_{Mg} + \gamma(Mg_{17}Al_{12})$ type (Fig. 10, Fig. 11, Tab. 5: point 2 and 4), the element concentration changes within the range of: 85.6÷89.4% Mg and 10.6÷14.0% Al, 0÷0.4% Si, respectively.

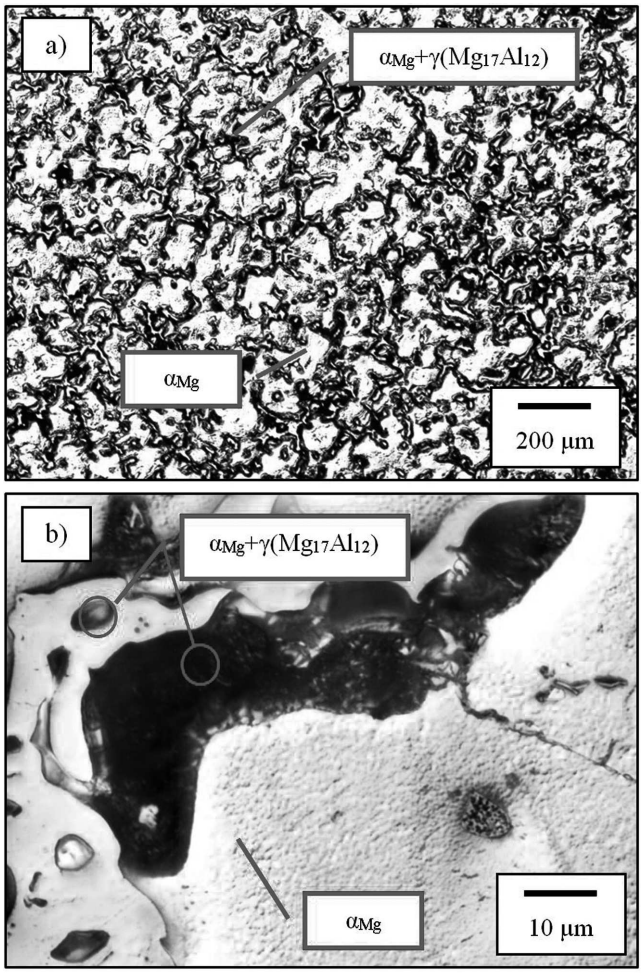

Fig. 9. Microstructure of the AZ91 alloy solidifying in the ceramic TDA sampler

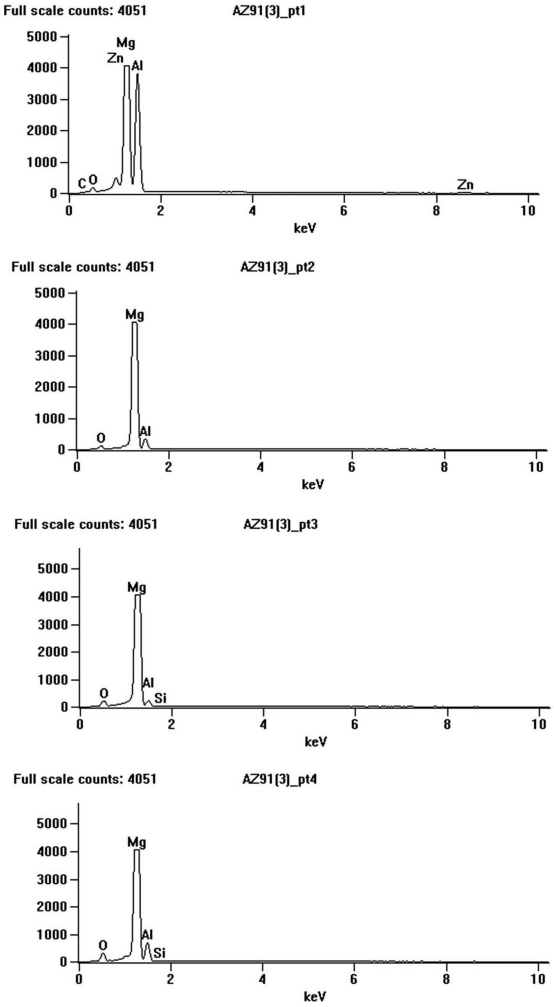

Fig. 11. Diagram of the chemical composition analysis at points 1–5 of the microstructure of the AZ91 alloy solidifying in the ceramic ATD10C-PŁsampler

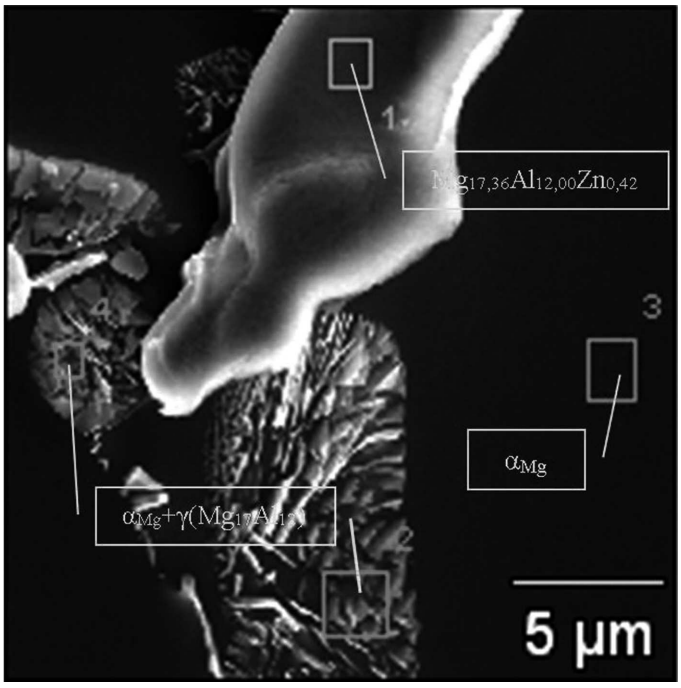

Fig. 10. Electron microscope photograph of the AZ91 alloy solidifying in the ceramic ATD10C-PŁsampler

TABLE 5

Results of the chemical composition analysis of the phases in the AZ91 alloy

Point of analysis	Element	Element concentration, %	
		Mass	Atomic
1	Mg	54.6	58.3
	Al	41.9	40.3
	Si	–	–
	Zn	3.5	1.4
2	Mg	89.4	90.4
	Al	10.6	9.6
	Si	–	–
	Zn	–	–
3	Mg	95.3	95.8
	Al	4.4	4.0
	Si	0.3	0.2
	Zn	–	–
4	Mg	85.6	86.9
	Al	14.0	12.8
	Si	0.4	0.3
	Zn	–	–

4. Conclusions

From the tests presented in this work, we can conclude that:

- the ceramic ATD10C-PŁsampler used in the research makes it possible to examine the crystallisation and solidification processes of the casts under the conditions similar to those occurring in the actual ceramic shells used in the preparation of casts by the investment casting method (lost wax method),
- the recorded thermal effects by the TDA method were confirmed by the presence of intermetallic phases in the tests performed by means of optical microscopy and scanning microscopy with an EDS analyser,
- the α_{Mg} phase crystallizes as first, followed by the intermetallic phases (depending on the type of the alloy, e.g.: AlMnMgSi, MgSi, MgAlZn) and the last to crystallize is the $\alpha_{Mg} + \gamma(Mg_{17}Al_{12})$ eutectic,
- there is a possibility to apply and implement the TDA method to control the quality of the liquid metal in foundries which produce casts made of alloys with a magnesium matrix.

Acknowledgements

This work was realized within the frames of Project PBS I, financed by the National Centre for Research and Development, Poland. Project ID: 178739. Project implemented in 2013-2015.

REFERENCES

[1] G. Gumienny, Carbidie Bainitic and Ausferritic Ductile Cast Iron. Archives of Metallurgy and Materials **58**(4), 1053-1058 (2013).

[2] G. Gumienny, Bainitic-martensitic nodular cast iron with carbides, Archives of Foundry Engineering **10**, 2, 63-68 (2010).

[3] S. Pietrowski, B. Pisarek, Computer-aided technology of melting high-quality metal alloys, Archives of Metallurgy And Materials **52**, 3, 481-486 (2007).

[4] B. Pisarek, Influence of the technology of melting and inoculation preliminary alloy AlBe5 on change of concentration of Al and micro-structure of the bronze CuAl10Ni5Fe4. Archives of Foundry Engineering **10**, 2, 127-134 (2010).

[5] S. Jura, Z. Jura, Theory of ATD method in tests of Al alloys, Solidification of Metals and Alloys **28**, PAN Katowice, 57-88 (1996) (in Polish).

[6] R. Wladysiak, Effect of water mist on cooling process of casting die and microstructure of AlSi11 alloy, Archives of Metallurgy and Materials **55**(3), 939-946 (2010).

[7] S. Pietrowski, T. Szymczak, Crystallisation, microstructure and mechanical properties of silumins with micro-additions of Cr, Mo, W and V, Archives of Foundry Engineering **10**, 1, 123-136 (2010).

[8] L.A. Dobrzański, T. Tański, A.D. Dobrzańska-Danikiewicz, M. Król, S. Malara, J. Domagała-Dubiel, The microstructure and properties of alloys of Mg-Al-Zn, Chapter 3 The derivative thermal analysis of Mg-Al-Zn Open Access Library **5** (11), 44-77 (2012) (in Polish).

[9] B. Nami, S.G. Shabestaria, S.M. Miresmaeili, H. Razavi, Sh. Mirdamadi, The effect of rare earth elements on the kinetics of the isothermal coarsening of the globular solid phase in semisolid AZ91 alloy produced via SIMA process, Journal of Alloys and Compounds **489**, 570-575 (2010).

[10] S. Lun Sin, D. Dubé, R. Tremblay, An investigation on microstructural and mechanical properties of solid mould investment casting of AZ91D magnesium alloy, Materials Characterization **59**, 178-187 (2008).

[11] H. Jafari, M.H. Idris, A. Ourdjini, M.R. Abdul Kadir, Effect of Flux on In-Situ Melting Shell Investment Casting of AZ91D Magnesium Alloy, International Conference on Thermal, Material and Mechanical Engineering (ICTMME'2012) July 15-16, Singapore, 143-148 (2012).

[12] Y. Zhiyong, Z. Yuhua, Ch. Weili, Z. Jinshan, W. Yinghui, Effect of Cu addition on microstructure and properties of Mg-10Zn-5Al-0.1Sb high zinc magnesium alloy, China Foundry, Research & Development, February, 43-47 (2012).

[13] S. Pietrowski, C. Rapiejko, Temperature and microstructure characteristics of silumin casting AlSi9 made with investment casting method, Archives of Foundry Engineering **11**, 3, 177-186 (2011).

[14] A. Maltais, D. Dube, M. Fiset, G. Laroche, S. Turgeon, Improvements in the metallography of as-cast AZ91 alloy, Material Characterization **52**, 103-119 (2004).

Received: 20 December 2013.